HEPATOLOGY

HEPATOLOGY, VOL. 74, NO. 5, 2021

YAP/TAZ Suppress Drug Penetration Into Hepatocellular Carcinoma Through Stromal Activation

Kyungjoo Cho,[1,2*] Simon Weonsang Ro,[3*] Hye Won Lee,[2,4] Hyuk Moon,[3] Sojung Han,[2,4] Hye Rim Kim,[5] Sang Hoon Ahn,[2,4] Jun Yong Park ,[1,2,4] and Do Young Kim[2,4]

BACKGROUND AND AIMS: HCC is the most predominant type of liver cancer affecting 800,000 people globally each year. Various small-molecule compounds targeting diverse oncogenic signaling pathways have been tested for patients with HCC, and clinical outcomes were not satisfactory. In this study, we investigated molecular signaling that determines the efficiency of drug delivery into HCC.

APPROACH AND RESULTS: Hydrodynamics-based transfection (HT) was performed to develop mouse models for HCC induced by various oncogenes. Mice bearing liver cancer were treated with verteporfin at 5 weeks after HT. Multicellular HCC organoid (MCHO) models were established that contained various types of stromal cells, such as hepatic stellate cells, fibroblasts, and endothelial cells together with HCC cells. Tumor organoids were treated with verteporfin, and distributions of the drug in the organoids were assessed using fluorescence microscopy. Murine HCC models developed by HT methods showed that a high Yes-associated protein/Transcriptional co-activator with PDZ-binding motif (YAP/TAZ) activity in HCC cells impaired verteporfin penetration into the cancer. Activation of tumor stroma was observed in HCC with a high YAP/TAZ activity. Consistent with the findings in the *in vivo* models of HCC, MCHOs with activated YAP/TAZ signaling showed stromal activation and impaired penetration of verteporfin into the tumor organoids. Inhibition of YAP/TAZ transcriptional activity in HCC cells significantly increased drug penetration into the MCHO.

CONCLUSIONS: Drug delivery into liver cancer is impaired by YAP/TAZ signaling in tumor cells and subsequent activation of stroma by the signaling. Disrupting or targeting activated tumor stroma might improve drug delivery into HCC with an elevated YAP/TAZ activity. (HEPATOLOGY 2021;74:2605-2621).

HCC is the most common type of liver cancer, accounting for about 80% of cases. The last decade has seen great advances in molecular targeted therapy for HCC.[1–3] Various small-molecule compounds targeting diverse oncogenic signaling pathways have been tested in preclinical and clinical settings. To date, however, clinical outcomes have been somewhat discouraging, as exemplified by sorafenib, the leading molecular target compound administered to patients with HCC. The mean survival benefit for sorafenib-treated groups compared with placebo groups is ~2-3 months.[4,5] Thus, development of target therapeutics is needed to improve treatment outcomes.

The transcription factors YAP and its paralogue TAZ have attracted considerable recent attention in cancer research.[6,7] Studies have identified central roles for YAP/TAZ in tumor initiation and maintenance as well

Abbreviations: α-SMA, alpha-smooth muscle actin; c-Myc, cellular myelocytomatosis oncogene; EGFP, enhanced green fluorescent protein; FBS, fetal bovine serum; GFP, green fluorescent protein; Hras, harvey rat sarcoma viral oncogene homolog; HUVEC, human umbilical vein endothelial cell; IHC, immunohistochemistry; MCHO, multicellular HCC organoid; PI3K, phosphoinositide 3-kinase; qPCR, quantitative PCR; SB, sleeping beauty; shRNA, short hairpin RNA; Smad7, mothers against decapentaplegic homolog 7; TAZ, Transcriptional co-activator with PDZ-binding motif; Tead2, TEA domain family member 2; Tead2dn, dominant-negative form of Tead2; VP, verteporfin; YAP, Yes-associated protein.

Received September 5, 2020; accepted May 22, 2021.

Additional Supporting Information may be found at onlinelibrary.wiley.com/doi/10.1002/hep.32000/suppinfo.

**These authors contributed equally to this work.*

Supported by the National Research Foundation of Korea (NRF) grant funded by the Korean government (MSIT) (NRF-2018R1A2B2005901 and 2017R1C1B2007770). The funders had no role in study design, data collection and analysis, decision to publish, or preparation of the manuscript.

View this article online at wileyonlinelibrary.com.

DOI 10.1002/hep.32000

Potential conflict of interest: Nothing to report.

as resistance to targeted therapies in a variety of cancers. Thus, targeting YAP/TAZ has emerged a promising therapeutic option either alone or in combination with other targeted therapies. YAP/TAZ induce dedifferentiation of hepatocytes, allowing them to manifest progenitor-like phenotypes.[8–12] Notably, YAP/TAZ signaling is activated in about 70% of human HCC, and activated YAP/TAZ in HCC is significantly correlated with poor prognosis.[13] Importantly, activation of YAP/TAZ signaling renders tumor cells resistant to rat sarcoma virus (RAS)-targeted or rapidly accelerated fibrosarcoma (RAF)-targeted therapies in pancreatic and lung cancers, blunting the efficacy of these targeted therapies or causing cancer relapse after an initial positive response.[6,14]

The tumor microenvironment is intimately involved in multiple facets of tumorigenesis, including tumor initiation, maintenance, migration, and metastasis.[15] It can also significantly affect the efficacy of chemotherapy. For example, accumulated extracellular matrix proteins and disorganized vessel structures can decrease drug delivery to the cancer, reducing tumoricidal effects.[16] Furthermore, aberrant production of growth factors and inflammatory cytokines in the tumor microenvironment can diminish the efficacy of a given targeted therapy by reactivating the targeted signaling pathway or inducing an alternative oncogenic signaling pathway in cancer cells.[17,18] A better understanding of how the tumor microenvironment affects the delivery and efficacy of cancer chemotherapeutics should lead to improved responses to cancer-targeted therapy.

In this study, we investigated *in vivo* therapeutic effects of the small-molecule YAP/TAZ inhibitors, verteporfin (VP) and CA3, employing a murine autochthonous HCC model developed using the hydrodynamic transfection method and the sleeping beauty (SB) transposon system.[19,20] Furthermore, to understand the mechanism responsible for suppressing drug penetration into tumors, we used multicellular HCC organoid (MCHO) models, in which liver stromal cells are cultured together with tumor cells, thus simulating the *in vivo* tumor microenvironment.

Materials and Methods

ANIMAL MODELS AND CLINICAL SPECIMENS

All experiments using mice were approved by the Animal Policy and Welfare Committee of the Yonsei University College of Medicine (permit numbers: 2019-0214 and 2020-0095). Wild-type male C57BL/6 mice were purchased from Orient Bio (Korea). Animals were housed in an animal facility under a 12-hour light/dark cycle and were provided food and water *ad libitum*. Human primary HCC tissues were obtained from a biobank at Severance Hospital, Seoul, Korea. Tissues were collected immediately following the operation and stored at -80°C until processing and use. This study was approved by the Independent Institutional Review Board of Severance Hospital (IRB number: 4-2018-1087) and conforms to the ethical guidelines of the 1975 Declaration of Helsinki. No donor organs were

ARTICLE INFORMATION:

From the [1]Brain Korea 21 Project for Medical Science College of Medicine, Yonsei University, Seoul, Korea; [2]Yonsei Liver Center, Yonsei University College of Medicine, Seoul, Korea; [3]Department of Genetics and Biotechnology, College of Life Sciences, Kyung Hee University, Yongin-si, Gyeonggi-do, Korea; [4]Department of Internal Medicine, Institute of Gastroenterology, Yonsei University College of Medicine, Seoul, Korea; [5]Biostatistics Collaboration Unit, Department of Biomedical Systems Informatics, Yonsei University College of Medicine, Seoul, Korea.

ADDRESS CORRESPONDENCE AND REPRINT REQUESTS TO:

Jun Yong Park, M.D., Ph.D.
Department of Internal Medicine, Severance Hospital
Yonsei University College of Medicine
50-1 Yonsei-ro, Seodaemun-gu
03722 Seoul, Korea
E-mail: DRPJY@yuhs.ac
Tel.: +1-82-2-2228-1988
or

Do Young Kim, M.D., Ph.D.
Department of Internal Medicine, Severance Hospital
Yonsei University College of Medicine
50-1 Yonsei-ro, Seodaemun-gu
Seoul 03722, Korea
E-mail: DYK1025@yuhs.ac
Tel.: +1-82-2-2228-1992

obtained from executed prisoners or other institutionalized persons.

CELL LINES AND CULTURE CONDITIONS

SNU449, SNU3059, SNU3160, and Hep3B human HCC cell lines and WI38 human fibroblast cells were obtained from the Korean Cell Line Bank. LX2 (human HSCs) were kindly provided by Dr. HaengRan Seo (Institut Pasteur Korea). Human umbilical vein endothelial cells (HUVECs) were obtained from Lonza (Switzerland). SNU449, SNU3059, and SNU3160 HCC cell lines cells were cultured in Roswell Park Memorial Institute (RPMI)-1640 medium (Gibco) and Hep3B HCC cell lines were cultured in minimum essential medium (Gibco) supplemented with 10% fetal bovine serum (FBS; Gibco). LX2 cells were maintained in DMEM (Gibco) supplemented with GlutaMAX and 2% FBS (Gibco) (complete media). WI38 cells were cultivated in RPMI-1640 medium (Gibco) supplemented with 10% FBS and 1× nonessential amino acids (Gibco). HUVECs were cultured in endothelial basal medium (Lonza).

HYDRODYNAMIC TRANSFECTION AND DRUG TREATMENT

The plasmids pT3/EF5a-TAZ^{S89A}, pT2/harvey rat sarcoma viral oncogene homolog (HRAS)^{G12V}, pT2/mothers against decapentaplegic homolog 7 (Smad7)-2A-Hras^{G12V}, pT2/cellular myelocytomatosis oncogene (c-Myc), pT2/shp53-green fluorescent protein (GFP) 4, pT2/enhanced green fluorescent protein (EGFP), and pPGK-SB13 were described.[21,22] Hydrodynamic injection has also been described.[21] DNA mixtures of transposons (pT2- or pT3- plasmids) and transposase-encoding vector (pPGK-SB13) were suspended in lactated Ringer's solution and subsequently injected into the lateral tail veins of male 5-6-week-old mice (0.1 mL/g body weight). Mice were randomly assigned to hydrodynamic injection. Drugs were intraperitoneally administered daily beginning 5 weeks after hydrodynamic transfection. Doses of drugs administered were 50 mg/kg/day for VP, 1 mg/kg/day for CA3 and 2 mg/kg/day for omipalisib. All drugs were purchased from Selleckchem. All mice in the control group received an equal volume of PBS (Welgene, Korea) by intraperitoneal injection according to the same treatment schedule.

IMAGING OF VP FLUORESCENCE IN HCC

Mouse livers were fixed by intracardiac perfusion with 4% paraformaldehyde and postfixed overnight at 4°C using the same solution. Tissues were cut into 100-μm-thick sections using a Leica VT1200S vibratome (Leica Biosystems, Germany). Liver samples were mounted with Fluoromount-G and imaged using an upright multiphoton laser-scanning microscope (Zeiss LSM 780) equipped with a ×20 objective (1,024 × 1,024 resolution). Mean of VP fluorescence intensity was quantified in regions of interest of equal area in control and VP-treated samples using Zeiss software, as described.[23] VP autofluorescence was detected using an inverted Zeiss laser-scanning microscope (LSM780) equipped with 425-440 nm excitation and 700-730 nm emission filter sets. Images were captured in a 10-μm stack and taken under the same objective for constant image scale/resolution for each experiment.

GENERATION OF MCHO MODELS AND VISUALIZATION OF DRUG PENETRATION

MCHO models containing various cell types were generated by mixing HCC cells and stromal cells (LX2, WI38, and HUVECs) at a 1:1 ratio and then seeding them at a density of 6×10^3 cells/well in 96-well, round-bottom, ultralow-attachment (ULA) microplates (Corning B.V. Life Sciences, the Netherlands). After formation of MCHO models, the viability of MCHO models following drug treatment was determined using a CellTiter-Glo 3D cell viability assay (Promega, Madison, WI). For imaging of drug penetration, organoids were treated with 10 μM VP for 30 minutes, 1 hour, and 12 hours. Organoids were fixed in 4% paraformaldehyde (T&I, Korea) for 20 minutes, and washed twice with PBS (Welgene). Subsequently, spheroids were transferred to Nunc Chamber Slides (Thermo Fisher Scientific) and covered in Fluoromount-G (Thermo Fisher Scientific). For analysis of VP penetration by fluorescent imaging, the major and minor axes of the spheroid are measured and fluorescent intensity for each distance (r/R; the ratio of distance from start point) using ZEN 2.3 SP1 (black edition, Zeiss). The major axis is defined as the line segment connecting a single pair of the farthest points on the contour and the minor axis is defined as the shortest line. The integrated

pixel intensity within the area was then normalized by spheroid area, and baseline fluorescence from spheroids not exposed to fluorescent drug was subtracted from the normalized signal. Samples were run in triplicate, and at least five independent measurement of spheroid were analyzed for each sample.

RECOMBINANT RETROVIRAL INFECTION AND SHORT HAIRPIN RNA TREATMENT

Retroviral vectors for human pQCXIN-EGFP, pQCXIN-YAP, pQCXIN–dominant-negative form of Tead2 (Tead2dn), pQCXIN-citrine, pQCXIN-mKate2, and pQCXIN-Cerulean were generated, and the resultant plasmids were transformed into *Escherichia coli* DH5α, purified, and cotransfected with the pVSV-G vector in the Retro-X Universal Packaging System (Clontech Laboratories, Inc.) using the pantropic GP2-293 packaging cell line (Clontech Laboratories, Inc.). Conditioned medium containing the virus was collected from each packaging cell culture within 24-48 hours after transfection. Viral titers were determined according to the procedure provided by the vendor. Cells were infected by incubating with conditioned medium containing viruses. For selection of retroviral vector-gene-expressing cells, each infected cell line (as HCC cell lines with citrine, LX2 and WI38 cells with mKate2, and HUVEC with Cerulean) was grown in the presence of G418 for 3 weeks. For retroviral vector-overexpressing cells, infected cells were grown in the presence of G418. Individual drug-resistant clones were collected, pooled, and expanded. For the short hairpin RNA (shRNA) study, the complementary DNA (cDNA) sequence of TAZ was obtained from GenBank (NM_015472). Four TAZ-specific shRNAs were designed based on rules described elsewhere.[24] As shown in Supporting Table S1, shRNA-expressing plasmids specifically targeting TAZ (termed TAZ-shRNA-a, b, c, and d) were constructed by GenePharma Corp. (Shanghai, China) using the pGPH1/GFP/Neo vector and expression of TAZ was determined by Western blotting.

LIVER HARVESTING AND TISSUE PROCESSING

Mice were deeply anesthetized by intraperitoneal injection of Zoletil (30 mg/kg) and xylazine (10 mg/kg). A midline laparotomy incision was performed, and livers were removed, photographed, and fixed. Human tumor tissue samples were collected freshly from the operating theater and then fixed in 4% paraformaldehyde. Fixed tissue samples were embedded in paraffin and serially sectioned into 4-μm-thick slices. Slices were stained with hematoxylin and eosin and picrosirius red following standard protocols. Liver lesions were assessed in accordance with the criteria established by Frith et al.[25]

IMMUNOHISTOCHEMICAL ANALYSES OF MOUSE AND HUMAN TISSUE SAMPLES

For immunohistochemistry (IHC), paraffin-embedded sections were deparaffinized in xylene and rehydrated in a decreasing graded ethanol series. Antigen epitopes were then unmasked using a 10 mM sodium citrate buffer (pH 6.0) incubation procedure, after which sections were incubated overnight at 4°C with the primary antibodies. For a full list of primary antibodies, see Supporting Table S2. After incubation with primary antibodies, sections were incubated with the appropriate biotinylated secondary antibody, followed by treatment with freshly prepared 3,3´-diaminobenzidine substrates (Vector Laboratories). Sections were lightly counterstained with hematoxylin and mounted.

RNA PURIFICATION AND REVERSE-TRANSCRIPTION AND REAL-TIME PCR AMPLIFICATION

Total RNA from extracted livers and cells was collected and purified with an RNeasy Mini Kit (Qiagen, Germany) and converted to cDNA using a Superscript IV Synthesis Kit (Invitrogen). Quantitative PCR (qPCR) was performed on a StepOnePlus PCR System using PCR master mix (Applied Biosystems, UK). The relative expression levels of target genes were normalized to glyceraldehyde 3-phosphate dehydrogenase levels. All qPCR results were obtained from at least three biological replicates. The sequences of the real-time PCR primers are provided in Supporting Table S3.

PROTEIN EXTRACTION AND WESTERN BLOTTING

Liver tissues and human MCHO cells were homogenized and digested in 1× radio immunoprecipitation

assay buffer containing a protease inhibitor and phosphatase inhibitor cocktail solution (Thermo Fisher Scientific). Western blotting experiments were performed following a standard protocol. For a full list of primary antibodies, see Supporting Table S1.

STATISTICAL ANALYSIS

Statistical analyses were carried out using two-tailed unpaired *t* tests and one-way ANOVA with Tukey's multiple-comparison *post hoc* test using GraphPad Prism Software. All values are expressed as means ± SEM of biological replicates. Statistical methods for comparing experimental groups in each experiment are indicated in the figure legends. Significant differences between two groups are denoted by asterisks (*P < 0.05; **P < 0.01; ***P < 0.001). In order to compare drug penetration, the difference of intensity according to drugs in each r/R was analyzed by permutation test (10,000 permutations). Assuming that values measured at different r/R are independent and values measured at the same r/R are paired, the paired-sample permutation test can determine whether there is a difference in drug intensity at the same r/R. Statistical significance was judged by comparing the values observed through experiments with values obtained through the permutation process. P value < 0.05 was considered statistically significant. Multiple comparisons were corrected using the Bonferroni method at the condition level. Statistical analyses were performed using R version 3.4.3 (The R Foundation for Statistical Computing, Austria).

Results

TREATMENT WITH YAP/TAZ INHIBITORS DOES NOT SUPPRESS TUMOR GROWTH IN A MURINE AUTOCHTHONOUS HCC MODEL

Employing a well-established liver-specific transgenic approach, we previously reported a murine HCC model in which HCC is induced by a constitutively active form of TAZ (TAZ^{S89A}) together with active RAS ($HRAS^{G12V}$). In this tumor model, HCC develops in adult mice as early as 5 weeks after oncogenic expression.[21,22] Because tumors are induced and maintained by activated YAP/TAZ signaling in this model, we presumed that any tumor-suppressive effects of YAP/TAZ inhibitors would be clearly manifested. Two small-molecule inhibitors, VP and CA3, which have been shown to effectively suppress the transcriptional activity of YAP/TAZ,[26,27] were used for YAP/TAZ targeted therapy in the HCC model.

Drug treatment was initiated 5 weeks after oncogene expression, at which time tumors had reached an average size of 1-2 mm in diameter (Fig. 1A). VP and CA3 were intraperitoneally administered daily at doses of 50 and 1 mg/kg, respectively, for 2 weeks. Reports have shown that intraperitoneal injection of VP at 50 mg/kg daily or at 100 mg/kg every other day for 2 weeks effectively suppressed tumor growth in murine xenograft models of various types of cancer, including HCC.[28–31] However, we found that treatment with VP at 50 mg/kg daily for 2 weeks did not suppress tumor growth in our autochthonous TAZ^{S89A}/$HRAS^{G12V}$-induced HCC model; treatment with CA3 was similarly ineffective (Fig. 1B). Neither the average number of tumors per liver nor mean tumor size was significantly different between drug-treated and vehicle-treated groups (Supporting Fig. S1).

Our first response to these findings was to question whether the drugs effectively suppressed TAZ signaling in tumors. An assessment of the expression levels of representative YAP/TAZ target genes revealed that both drugs failed to inhibit the transcriptional activity of YAP/TAZ in tumors (Fig. 1C and Supporting Fig. S2A). Likewise, neither VP nor CA3 suppressed nuclear accumulation of TAZ in tumor cells (Supporting Fig. S2B). To test whether VP can inhibit TAZ, we treated TAZ-overexpressing Hep3B cells with VP in two-dimensional cultures and assessed the expression levels of its target genes. The experiment showed that VP suppressed the gene expression in a dose-dependent manner (Supporting Fig. S2C). Thus, we speculated that the minimal effects of these drugs on tumor growth in our murine autochthonous HCC model were attributable to inefficient suppression of YAP/TAZ activity in tumors.

DELIVERY OF VP INTO HCC IS IMPAIRED

Although there are several possible explanations for the failure of VP and CA3 to inhibit TAZ in the TAZ^{S89A}/$HRAS^{G12V}$-induced murine model of HCC,

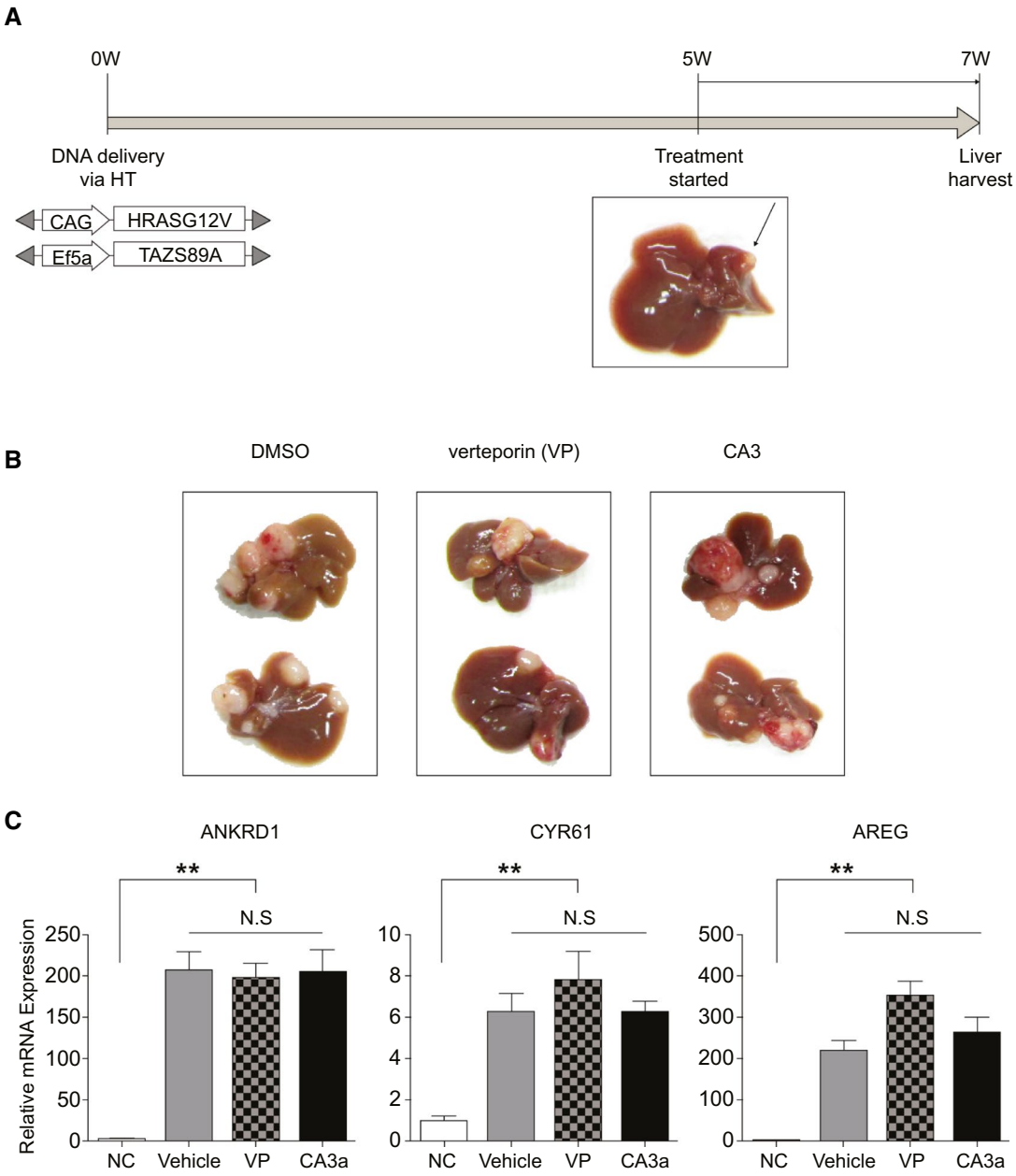

FIG. 1. Effects of YAP/TAZ inhibition on HCC. (A) Schematic illustration of the experimental procedure. Transposons encoding TAZ^{S89A} plus $HRAS^{G12V}$ were hydrodynamically delivered to the liver. Treatment with vehicle, VP, or CA3 was started at 5 weeks after hydrodynamics-based transfection (HT) and continued for 2 weeks. The gross morphology of a representative liver at 5 weeks after HT is shown. Arrow indicates a tumor in the liver. (B) Gross morphology of representative livers treated with each drug (n = 10 male C57BL/6 mice per group). (C) RT-qPCR assessment of the expression levels of YAP/TAZ target genes in tumors treated with each drug. Data are presented as means ± SEM (**$P < 0.01$). Abbreviation: ANKRD1, Ankyrin Repeat Domain 1; AREG, Amphiregulin; CYR61, Cysteine-rich angiogenic inducer 61; NC, normal control liver;.

we first considered the possibility that the YAP/TAZ inhibitors were not properly delivered into tumors. Drug delivery into tumors can be affected by various cellular and histological factors that undermine the efficacy of cancer therapeutic drugs.[32,33]

To address this issue, we sought to investigate the distribution of VP to tumor-bearing livers. VP is a benzoporphyrin derivative that exhibits red fluorescence on excitation at 420-440 nm, allowing the distribution and relative concentration of the drug within

tissue to be determined based on fluorescence intensity.[34,35] To better distinguish tumors from normal surrounding hepatic tissue, we codelivered a reporter gene encoding EGFP with the genes encoding TAZ^{S89A} and $HRAS^{G12V}$. This allows tumors to be genetically marked with EGFP (Fig. 2A). At 5 weeks posthydrodynamic transfection, mice were treated with a single 50 mg/kg dose of VP, and livers were harvested 4, 8, 12, and 24 hours after administration.

Laser-scanning confocal microscopic images of liver sections from VP-treated mice consistently revealed striking differences in VP florescence intensity between tumors and surrounding normal tissues, even 24 hours after VP treatment (Fig. 2B,C). The mean VP fluorescence intensity from tumor areas was ~4-fold lower than that from normal tissue areas up to 12 hours after treatment; this difference was reduced to ~2-fold in livers harvested 24 hours after drug treatment (Fig. 2C). These data show that the drug concentration in tumors was significantly lower than that in normal hepatic tissue, suggesting that VP did not efficiently penetrate into the tumor and thus exerted minimal effects on tumor cells. In livers of mice that had not been treated with VP, red fluorescence following excitation at 420-440 nm was virtually undetectable, ruling out the possibility that the red fluorescence observed in VP-treated livers was attributable to tissue autofluorescence (Supporting Fig. S3).

DRUG DELIVERY IS IMPAIRED IN HCC WITH HIGH YAP/TAZ ACTIVITY

Next, we wondered whether impaired delivery of drugs into tumors is a general feature of murine autochthonous models of HCC developed by the hydrodynamic transfection method. To address this, we used another HCC model developed by hydrodynamic transfection[22] in which HCC is induced by simultaneous expression of Smad7, $HRAS^{G12V}$, and c-Myc (hereafter, S7HM mice). At 5 weeks after hydrodynamic transfection, both S7HM mice and TAZ^{S89A} plus $HRAS^{G12V}$ mice (hereafter, TH mice) were treated with a single 50 mg/kg dose of VP, and their livers were harvested 8 hours after treatment. Consistent with the findings indicated above (Fig. 2B,C), fluorescence imaging of liver sections of TH mice showed that VP fluorescence was significantly lower in tumors than in surrounding normal tissues. However, livers of S7HM mice showed similar VP fluorescence intensities in tumors and normal tissues, suggesting that impaired delivery of VP into tumors is specific to the TAZ^{S89A} and $HRAS^{G12V}$-induced HCC model (Fig. 3A,B).

Because HCC in TH mice exhibit characteristically high levels of TAZ activity (Fig. 1C and Supporting Fig. S2), we were curious about TAZ activity levels in tumors of S7HM mice. IHC analyses showed that nuclear localization of TAZ was barely detectable in S7HM tumors, whereas strong nuclear TAZ staining was observed in TH tumors (Fig. 3C). Consistent with this, RT-qPCR analyses also showed that expression levels of the YAP/TAZ target genes, *Cysteine-rich angiogenic inducer 61*, *Ankyrin Repeat Domain 1*, and *Baculoviral IAP Repeat Containing 5*, in S7HM tumors were significantly lower than those in TH tumors and were comparable with those in normal liver tissues (Fig. 3D and Supporting Fig. S4A-F). These data suggest a possible relationship between impaired drug delivery into HCC and TAZ activity in the tumor. To investigate whether efficient penetration of VP into S7HM tumors can lead to tumor suppression, we treated S7HM mice with VP at 50 mg/kg daily for 2 weeks, the dose of which failed to suppress TH tumors (Fig. 1B). Tumor growth in S7HM mice, with low levels of YAP/TAZ activity, was efficiently inhibited by the treatment (Supporting Fig. S4G).

HCC WITH HIGH YAP/TAZ ACTIVITY SHOWS ACTIVATION OF THE TUMOR STROMA

One of the striking histological features of TAZ^{S89A} and $HRAS^{G12V}$-induced HCC is the extensive accumulation of collagen around and within the tumor (Fig. 3C). Collagen is primarily synthesized and secreted by activated HSCs, which contribute to stromal activation in the liver. To further investigate the stromal activation in tumors with elevated YAP/TAZ signaling, we assessed expression levels of various stromal activation markers such as alpha-smooth muscle actin (α-SMA), fibronectin, and vimentin in TH tumors (Fig. 3D and Supporting Fig. S4). RT-qPCR showed that expression levels of these markers were significantly higher in TH tumors than in S7HM tumors or normal control liver tissues. Of note, TGF-β and connective tissue growth factor (CTGF)—the master regulators of hepatic fibrosis—were significantly

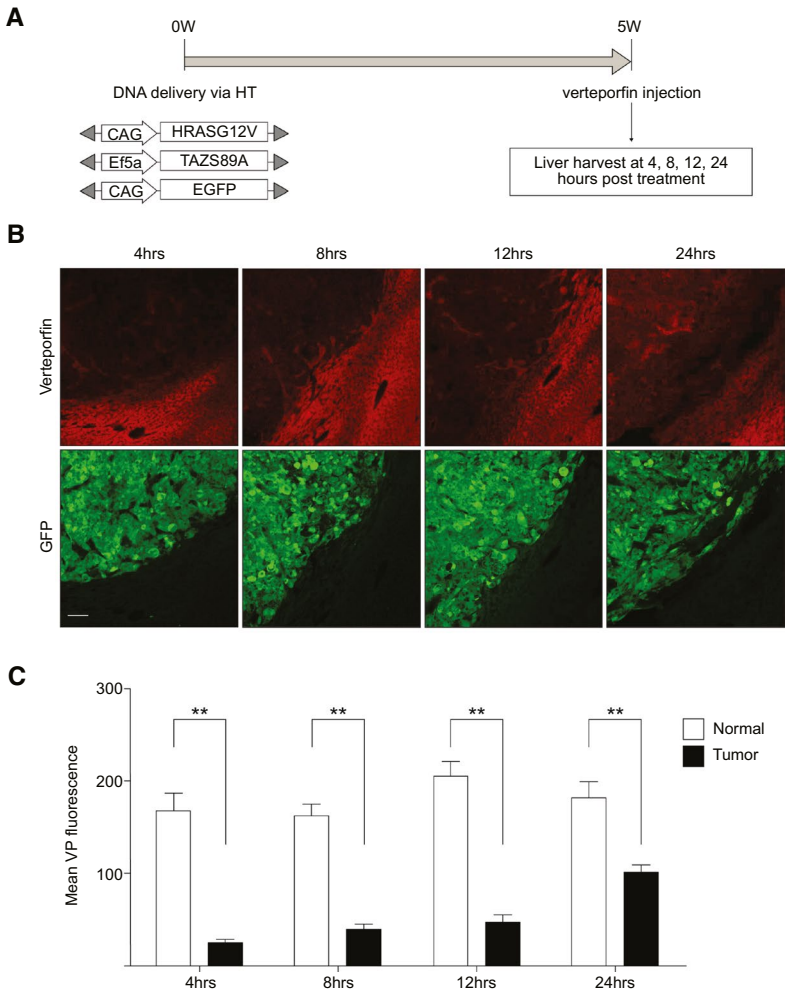

FIG. 2. Penetration of VP into HCC induced by $HRAS^{G12V}$ plus TAZ^{S89A}. (A) Schematic illustration of the experimental procedure. Transposons encoding $HRAS^{G12V}$, TAZ^{S89A}, and EGFP were codelivered to the liver. Five weeks after hydrodynamics-based transfection, mice were treated with VP, and livers were harvested 4, 8, 12, and 24 hours after treatment. (B) Images of VP fluorescence (upper panels) and EGFP fluorescence (lower panels) from livers that were harvested at the indicated time points after VP administration. Green fluorescence, reflecting expression of the EGFP reporter, corresponds to tumor areas. Scale bar, 100 μm. (C) Mean VP fluorescence in tumor and surrounding normal tissue areas at the indicated time points. $^{**}P < 0.01$. Abbreviation: HT, hydrodynamic transfection.

up-regulated in TH tumors (Supporting Fig. S4D,E). Consistent with this, IHC analyses and Western blotting showed that genes related to stromal activation were up-regulated in TH tumors compared with S7HM tumors and normal control liver tissues (Fig. 3C and E). In the context of TAZ expression-dependent drug penetration in HCCs, we examined whether TAZ activation affects stromal activation and ultimately regulates drug uptake. To test this, TAZ was ectopically expressed in S7HM tumors (referred to as S7HMT tumors). We delivered transposons encoding TAZ^{S89A} into murine livers together with transposons encoding Smad7, $HRAS^{G12V}$, and c-Myc through hydrodynamics-based transfection. At 5 weeks after hydrodynamic transfection, both S7HM mice and S7HMT mice were treated with VP, and their livers were harvested 8 hours posttreatment. Fluorescence imaging of liver sections from S7HMT mice showed significantly lower VP fluorescence in tumors than in surrounding normal tissues (Fig. 4A). Histological analysis revealed greater collagen deposition around and within tumors in S7HMT mice when compared with S7HM tumors (Fig. 4B). Stromal activation markers were also up-regulated in S7HMT tumors (Fig. 4C). Taken together, these results suggest that the impaired delivery of VP into

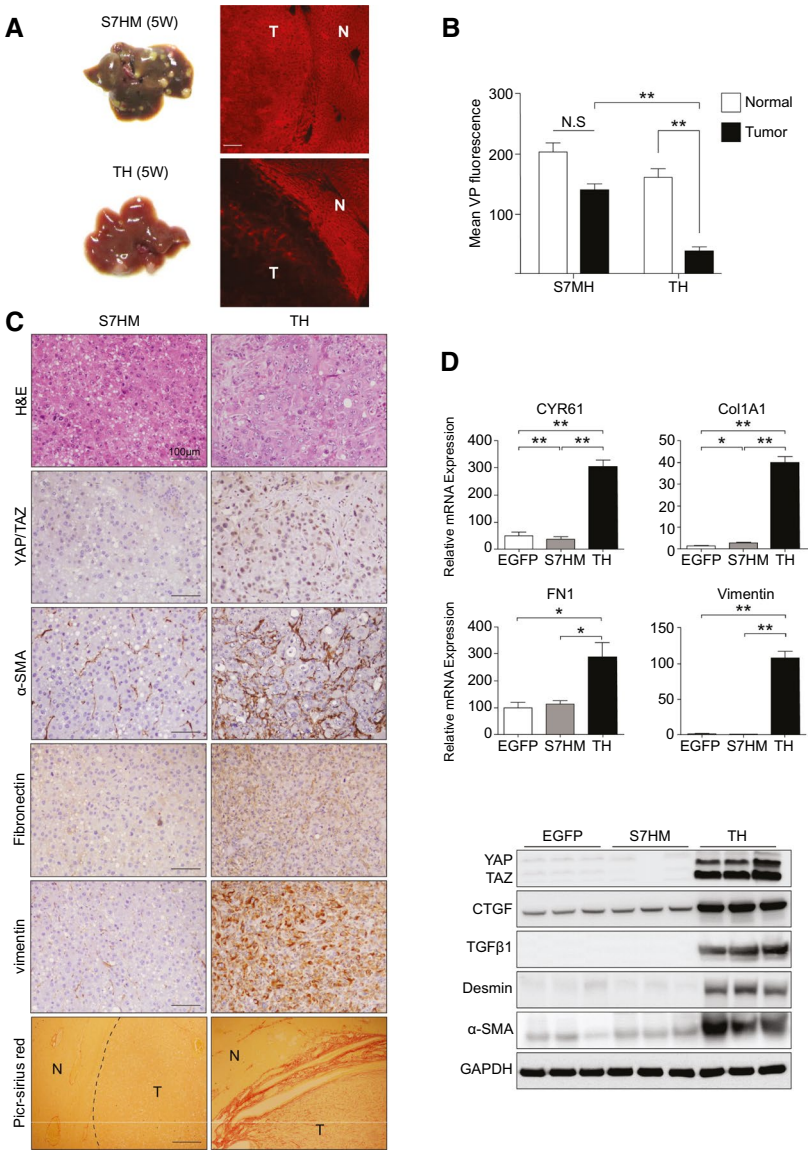

FIG. 3. Degrees of VP penetration into HCC with different levels of YAP/TAZ activity. (A) The gross morphology of representative livers of the indicated HCC models and images of VP fluorescence in the liver sections. T, tumor area; N, normal tissue area. Scale bar, 100 μm. (B) Mean VP fluorescence in tumor and surrounding normal tissue areas of each HCC model. (C) Hematoxylin and eosin (H&E) and IHC images of paraffin-embedded sections from S7HM and TH tumors. Scale bar, 50 μm. (D) RT-qPCR assessment of the expression levels of the indicated genes in S7HM and TH tumors. Livers hydrodynamically transfected with EGFP were used as controls. (E) Images of immunoblots showing expression levels of the indicated genes in each HCC model. Abbreviation: CYR61, Cysteine-rich angiogenic inducer 61; FN1, Fibronectin 1; GAPDH, glyceraldehyde 3-phosphate dehydrogenase. $^{**}P < 0.01$.

tumors can be attributable to TAZ activity in HCC and/or TAZ-induced stromal activation and extracellular matrix deposition.[36,37] To investigate whether high YAP/TAZ activity is correlated with activation of the tumor stroma in human HCC, we performed IHC staining for YAP/TAZ and picrosirius red staining for collagen. Extensive accumulation of collagen was found in human HCC with elevated YAP/TAZ expression, whereas deposition of collagen in human HCC with low YAP/TAZ activity was minimal (Fig. 4D). Consistent with these IHC results, Western blotting also showed a strong correlation between YAP/TAZ activity and stromal activation in human HCC (Fig. 4E). Thus, data from both murine and

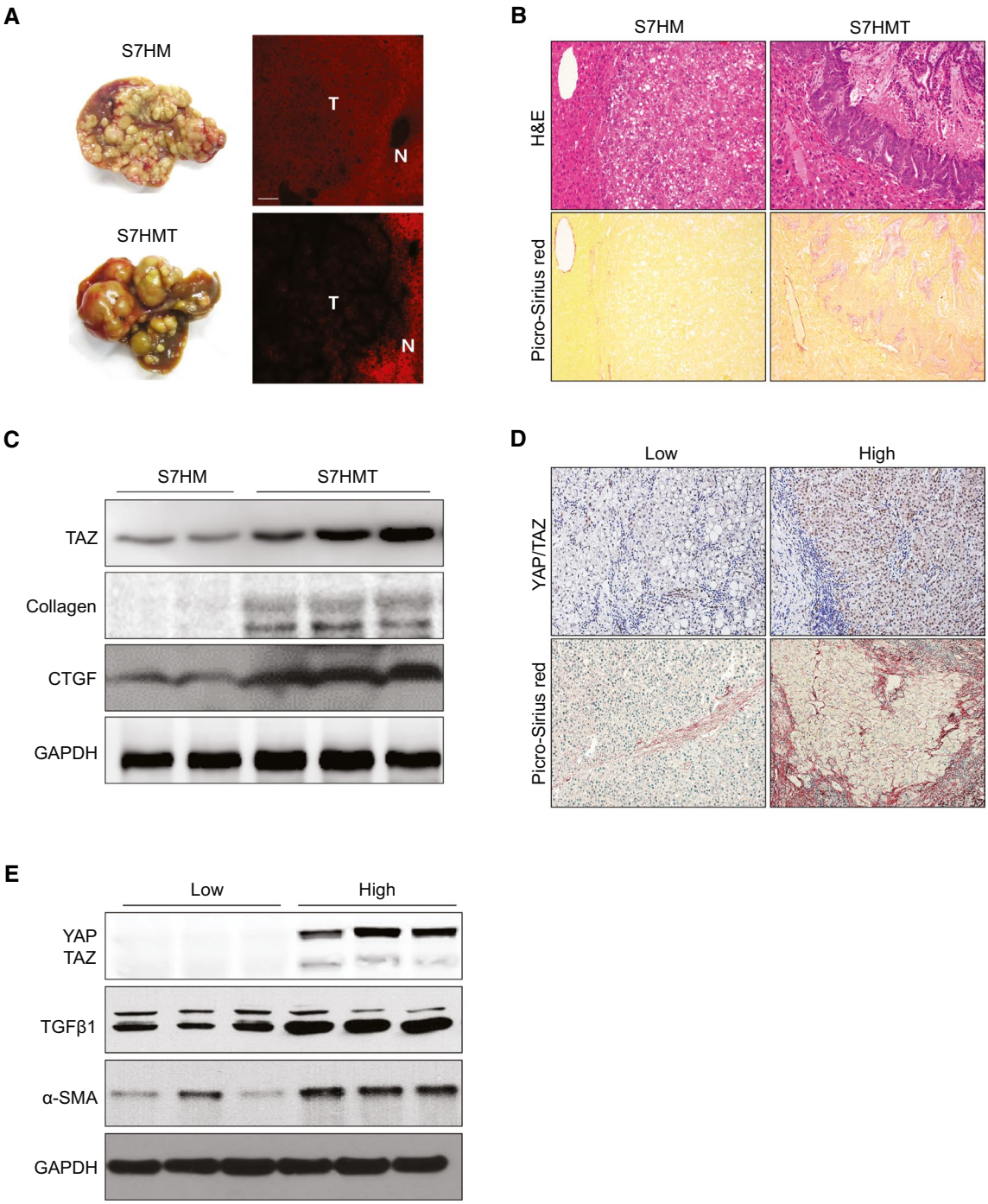

FIG. 4. Differential stromal activation in primary HCC tumors. (A) The gross morphology of representative livers of the indicated HCC models and images of VP fluorescence in liver sections. (B) Hematoxylin and eosin (H&E) and picrosirius red-stained images of paraffin-embedded sections from S7HM and S7HMT tumors. (C) Images of immunoblots showing expression levels of the indicated proteins in each HCC model. (D) IHC and picrosirius red-stained images of paraffin-embedded sections from human HCC samples. Scale bar, 100 μm. (E) Images of immunoblots showing expression levels of the indicated genes in each patient with HCC. Abbreviation: GAPDH, glyceraldehyde 3-phosphate dehydrogenase.

human HCC support the conclusion that tumors with elevated YAP/TAZ signaling exhibit an activated stroma.

OMIPALISIB FAILS TO SUPPRESS PHOSPHOINOSITIDE 3-KINASE ACTIVITY IN HCC WITH HIGH YAP/TAZ ACTIVITY

Having established that VP does not efficiently penetrate into TAZ^{S89A}/$HRAS^{G12V}$-induced HCC but is efficiently delivered into tumors with low YAP/TAZ activity (i.e., S7HM tumors; see Fig. 3A,B), we next considered whether the impaired delivery and efficacy of VP observed in TH tumors would also extend to clinically approved cancer therapeutics. Omipalisib is a potent phosphoinositide 3-kinase (PI3K) inhibitor that is used clinically as a targeted therapeutic for various types of cancer. Because both TH and S7HM tumors exhibited elevated levels of phosphorylated AKT (pAKT), an indicator of PI3K activation, we investigated the efficacy of PI3K inhibition by omipalisib in the two liver cancer models by assessing levels of pAKT. Although pAKT levels were significantly reduced in S7HM tumors following treatment with omipalisib (Fig. 5A), the same dose of the drug did not down-regulate pAKT levels in TH tumors (Fig. 5B). These data strongly suggest that the efficacy of cancer therapeutics can be significantly affected by the efficiency of drug delivery into the tumor.

ESTABLISHMENT OF MCHOS WITH DIFFERENT YAP/TAZ LEVELS

Next, we sought to elucidate the mechanism underlying the regulation of drug penetration into HCC. In particular, we were interested in determining whether YAP/TAZ activity in the tumor is casually related to drug penetration into the tumor. To this end, we established an MCHO model containing various types of stromal cells, including HSCs (LX2), fibroblasts (WI38), and endothelial cells (HUVEC), together with tumor cells (Fig. 6A). Four HCC cell lines (SNU449, SNU3059, SNU3160, and Hep3B) were individually mixed with stromal cells and cultured on V-shaped wells to form three-dimensional tumor organoids. For comparison, we generated

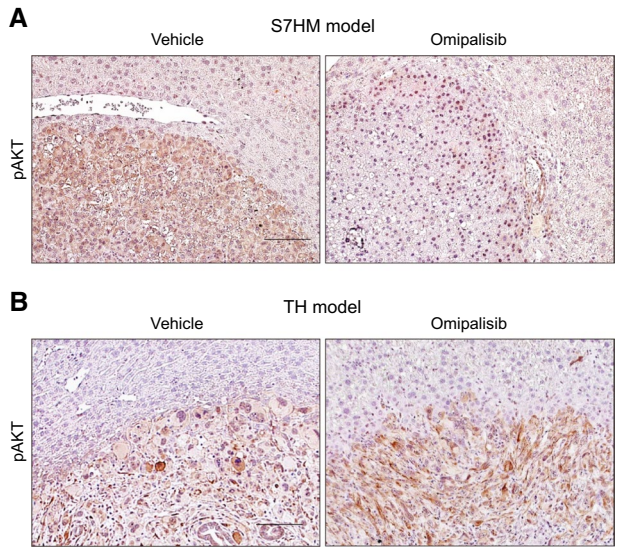

FIG. 5. Levels of pAKT in tumors from S7HM and TH models after treatment with the potent PI3K inhibitor, omipalisib. Representative IHC images showing pAKT levels in the (A) S7HM model and (B) TH model. Scale bar, 100 μm.

organoids containing only HCC cells (hereafter, HCC-only organoid). The addition of stromal cells led to a more compact organoid structure compared with that observed in HCC-only organoids (Fig. 6B).

We then investigated YAP/TAZ levels in each MCHO by Western blotting of whole cell extracts from MCHOs. These analyses revealed that the expression level of YAP/TAZ was highest in MCHOs containing Hep3B cells (Hep3B-MCHO), whereas those containing SNU449 cells (SNU449-MCHO) showed the lowest levels among the four types of MCHOs (Fig. 6C). In line with YAP/TAZ levels, expression of representative YAP/TAZ target genes was highest in Hep3B-MCHOs and lowest in SNU449-MCHOs (Fig. 6D). To investigate activation of the tumor stroma, we assessed expression levels of various genes involved in stromal activation in each MCHO. Hep3B-MCHOs showed the highest expression levels of major extracellular matrix proteins, such as collagen and fibronectin, as well as the fibrogenic cytokines, TGF-β and CTGF (Supporting Fig. S5A). Notably, mesenchymal genes also showed elevated expression in Hep3B-MCHOs (Supporting Fig. S5B).

To investigate distributions of HCC and stromal cells within organoids, we generated HCC cell lines stably expressing citrine (GFP), stromal cells (i.e.,

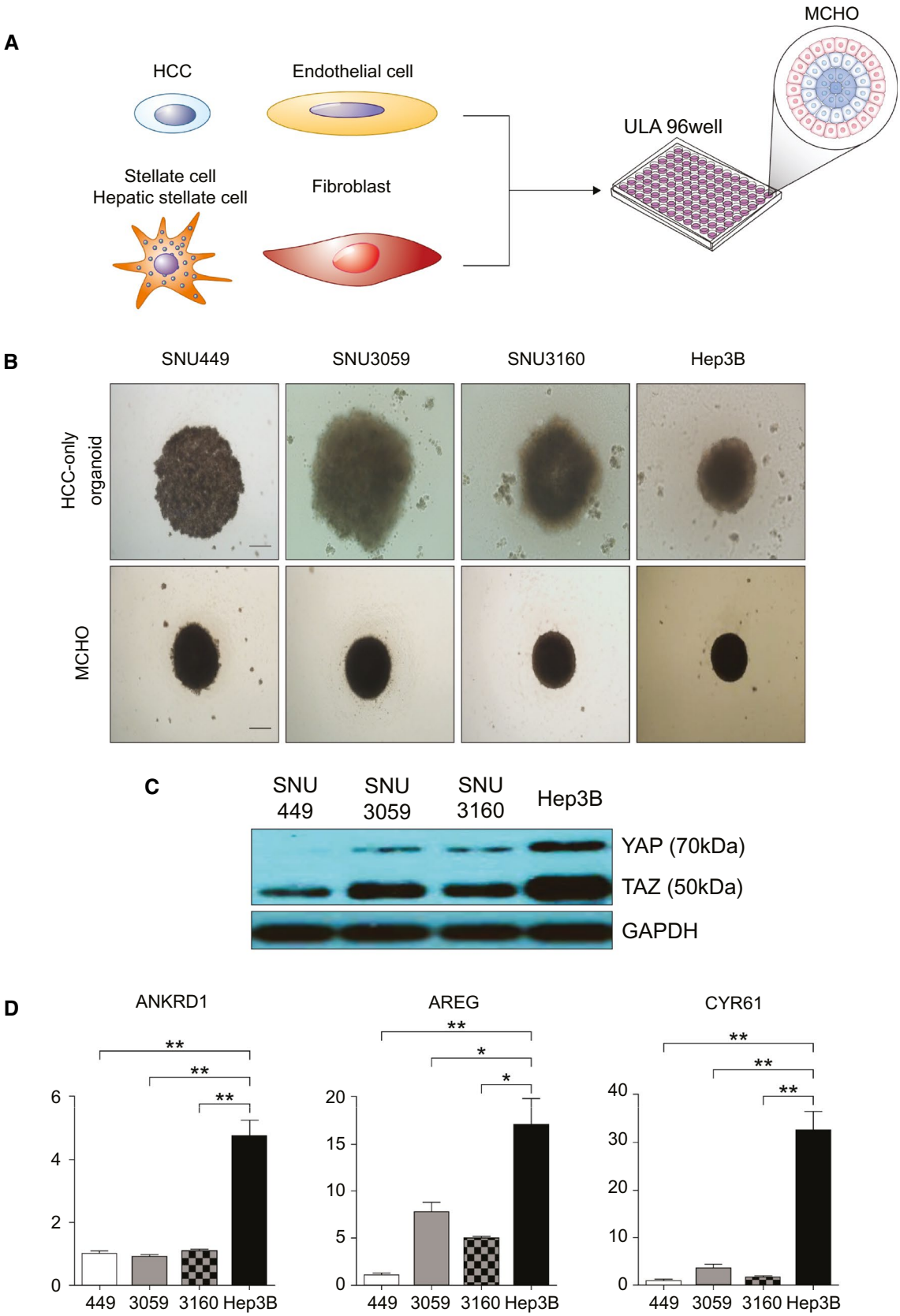
A
HCC
Endothelial cell
Stellate cell
Hepatic stellate cell
Fibroblast
ULA 96well
MCHO
B
SNU449
SNU3059
SNU3160
Hep3B
HCC-only organoid
MCHO
C
SNU 449
SNU 3059
SNU 3160
Hep3B
YAP (70kDa)
TAZ (50kDa)
GAPDH
D
ANKRD1
AREG
CYR61
449
3059
3160
Hep3B

FIG. 6. Establishment of MCHOs. (A) Illustration of the organoid model containing HCC cells and stromal cells. (B) Photographs of different HCC organoids with (bottom panels) and without (upper panels) stromal cells. Scale bar, 200 μm. (C) Expression levels of YAP and TAZ in the indicated MCHOs. Proteins in whole cell extracts from each MCHO were assessed by immunoblotting. (D) Quantification of mRNA expression levels of YAP/TAZ target genes in the indicated MCHOs. Abbreviation: GAPDH, glyceraldehyde 3-phosphate dehydrogenase; ANKRD1, Ankyrin Repeat Domain 1; AREG, Amphiregulin; CYR61, Cysteine-rich angiogenic inducer 61. $^{*}P < 0.05$, $^{**}P < 0.01$.

LX2 and WI38 cells) expressing mKate2 (red fluorescent protein), and HUVECs expressing Cerulean3 (blue fluorescent protein). We constructed SNU449-MCHOs and Hep3B-MCHOs using HCC cells and stromal cells expressing the fluorescent proteins. In both MCHOs, stromal cells surrounded HCC cells (Supporting Fig. S5C)

VP PENETRATION INTO HEP3B-MCHOS IS IMPAIRED

We studied penetration of VP into the various MCHOs at 1 and 12 hours after treating with the drug by direct imaging of organoids using laser-scanning confocal microscopy (Fig. 7A). Penetration of VP was significantly impaired in Hep3B-MCHOs, which exhibited fluorescence only in the exterior of organoids at 12 hours posttreatment. In contrast, SNU449-MCHOs exhibited strong, nearly ubiquitous VP fluorescence throughout the organoid at this same time point. Quantitative measurements of VP fluorescence revealed that the degree of VP penetration into Hep3B-MCHOs was significantly lower compared with penetration into other HCC-MCHOs (Fig. 7B and Supporting Table S4), especially SNU449-MCHOs. Considering that Hep3B-MCHOs exhibited the highest YAP/TAZ activity and SNU449-MCHOs the lowest, results from MCHO experiments are consistent with *in vivo* data in which HCC with high YAP/TAZ activity (i.e., TH mouse model) showed impaired VP penetration into tumors, whereas HCC with low YAP/TAZ activity (i.e., S7HM mouse model) exhibited high penetration of the drug (Fig. 3A,B). To rule out the possibility that drug uptake is intrinsically low or drug outflux is intrinsically high in Hep3B cells, we treated Hep3B and SNU449 cells with VP on a monolayer cell culture. As early as 30 minutes after treatment, VP was clearly detectable within Hep3B cells, and no difference in intracellular levels of VP was found between Hep3B and SNU449 cells (Supporting Fig. S6A). Investigation of occludin in MCHOs revealed that levels of the tight junction protein were higher in Hep3B-MCHO than those in SNU449-MCHO (Supporting Fig. S6B). The data imply that YAP/TAZ regulate the expression and rearrangement of tight junction proteins in tumor cells, which could function as barriers to drug penetration.[38]

YAP/TAZ SUPPRESSES DRUG PENETRATION INTO TUMOR

Because the degree of VP penetration into tumors correlated with YAP/TAZ activity in tumor cells in both *in vivo* mouse autochthonous models of HCC and *in vitro* human HCC organoid models, we wondered whether YAP/TAZ play a pivotal role in drug penetration. To test this possibility, we increased the activity of YAP in SNU449-MCHOs by ectopically expressing YAP in SNU449 cells while suppressing the activity of YAP/TAZ in Hep3B-MCHOs by overexpressing Tead2dn in Hep3B cells. VP fluorescence in organoids was directly imaged 12 hours after drug treatment using a laser-scanning confocal microscope. Overexpression of YAP in SNU449 cells significantly impeded drug penetration into SNU449-MCHOs (Fig. 7C and Supporting Table S5), whereas inhibition of YAP/TAZ transcriptional activity in Hep3B cells significantly increased drug penetration into Hep3B-MCHOs (Fig. 7D and Supporting Table S5). Consistent with this, drug uptake was significantly increased in short hairpin TAZ-Hep3B-MCHOs in which TAZ was down-regulated using shRNAs compared with Hep3B-MCHOs (Supporting Fig. S7 and Supporting Table S6). These data demonstrate that the activity of YAP/TAZ in tumor cells determines the degree of drug penetration into tumors.

STROMAL INTERACTIONS BY YAP/TAZ INFLUENCE DRUG PENETRATION

To investigate stromal effects of YAP/TAZ down-regulation in Hep3B-MCHOs, we compared expression levels of genes involved in stromal activation

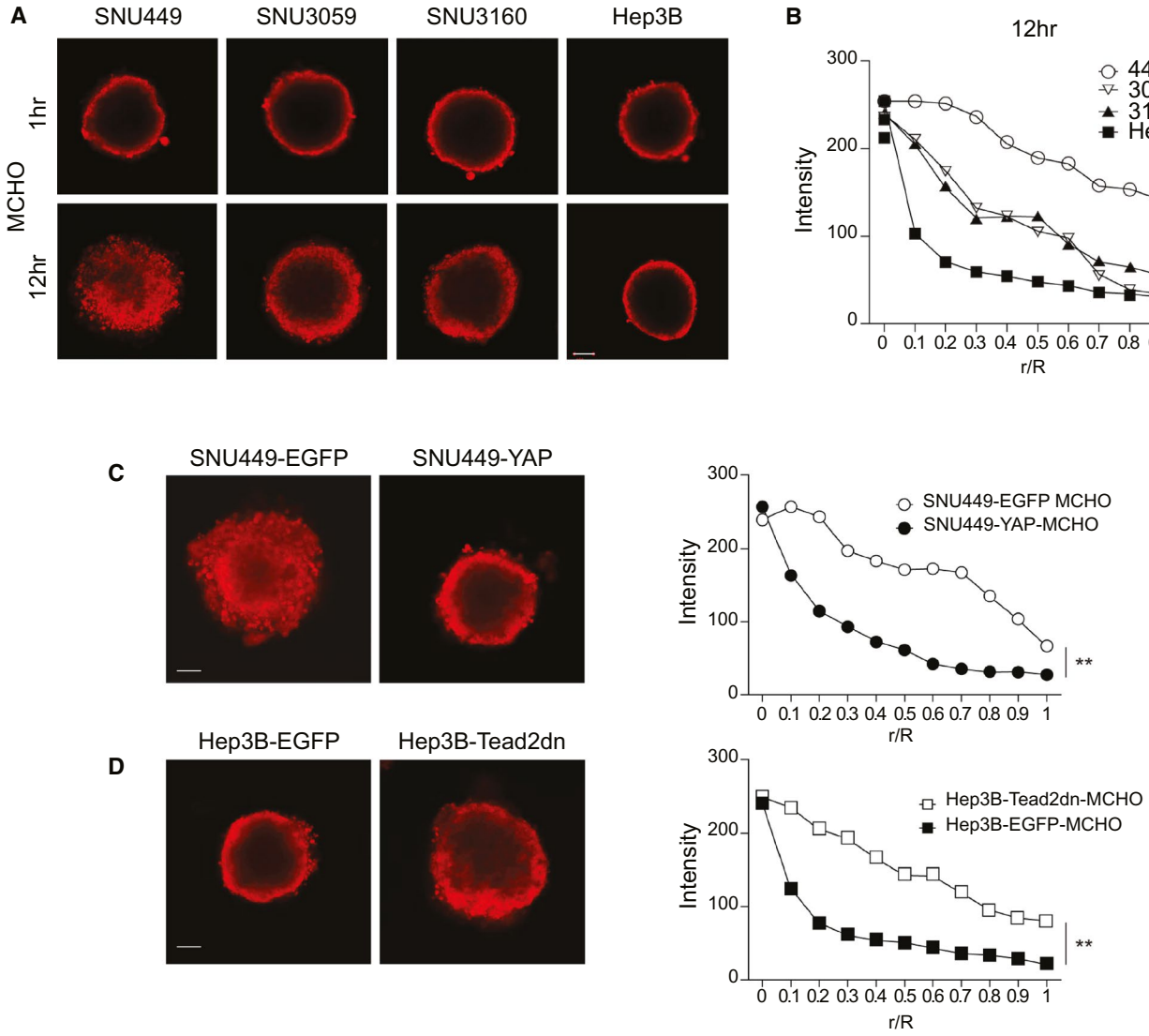

FIG. 7. VP penetration in MCHOs. (A) Each MCHO was treated with VP, and confocal fluorescence microscopy images were acquired 1 and 12 hours after treatment. Scale bar, 100 μm. (B) Graphical representation of mean VP fluorescence at the indicated depth of organoids. Depths are represented as *r*/*R*, where *R* is the radius of each organoid and *r* is the depth from the surface of the organoid. VP fluorescence at each depth of the organoid was measured 12 hours after treatment. (C,D) Images of VP fluorescence in each MCHO at 12 hours after treatment (left panels) and graphs showing mean VP fluorescence at the indicated depths in organoids (right panels). Scale bar, 100 μm. $^{*}P < 0.05$, $^{**}P < 0.01$.

between Hep3B-Tead2dn-MCHOs and Hep3B-EGFP-MCHOs (Supporting Fig. S8). Suppression of YAP/TAZ in Hep3B cells led to a significant decrease in expression levels of the stromal genes *α-SMA* and Collagen Type I Alpha 1 Chain (*Col1A1*) in MCHOs.

To determine the role of stromal activation by YAP/TAZ in drug penetration into tumors, we compared levels of VP penetration between Hep3B-MCHOs and Hep3B organoids without stromal cells (i.e., Hep3B-only organoids). Removing stromal cells from tumor organoids led to significantly increased penetration of VP into the tumor organoids (Fig. 8A). Of note, the degree of VP penetration into Hep3B-only organoids was comparable with that observed in

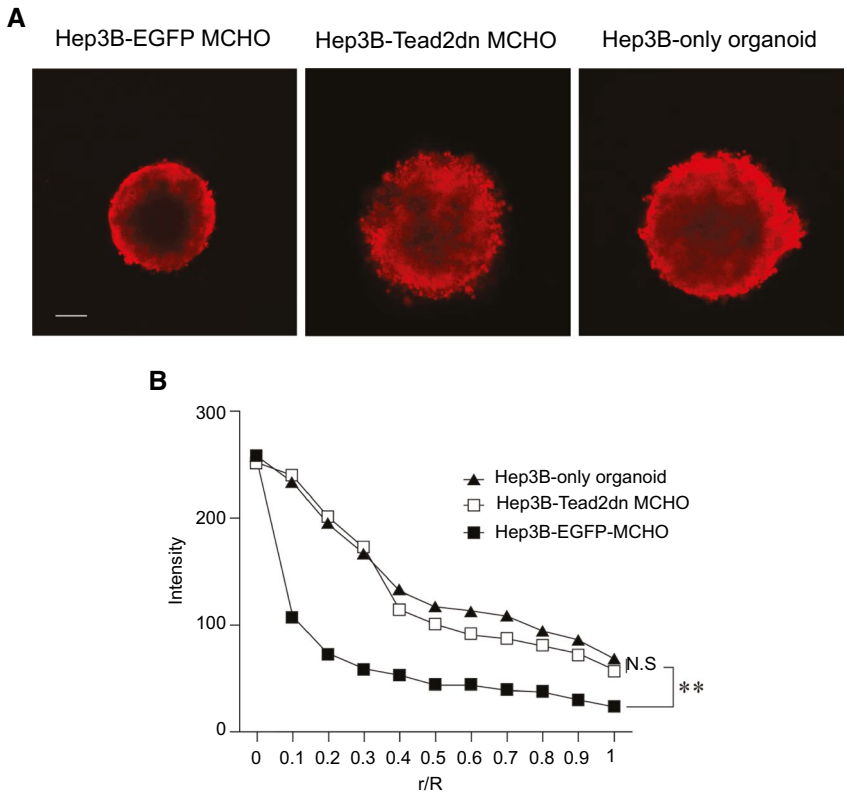

FIG. 8. VP penetration into Hep3B-MCHOs and Hep3B-only organoids. (A) Organoids were treated with VP, and images of VP fluorescence were acquired 12 hours after treatment. Scale bar, 100 μm. (B) Graphical representation of mean VP fluorescence along the depths (represented by *r*/*R*) of the indicated organoids 12 hours after treatment. $^{**}P < 0.01$.

Hep3B-Tead2dn-MCHOs (Fig. 8B and Supporting Table S7).

To determine the potential role of each type of stromal cell in drug penetration, we generated HCC organoids containing only one type of stromal cell, combinations of two types, and finally, all three types of stromal cells and then compared VP penetration in each organoid (Supporting Fig. S9A and S9B and Supporting Table S8). We found that WI38 cells (fibroblasts) played a more significant role in impeding drug penetration than endothelial cells or stellate cells. Considering that HCC organoids containing all three types of stromal cells showed the greatest impairment in drug penetration compared with other organoids, our inference is that each type of stromal cell contributes to the suppression of drug penetration. Western blotting showed a correlation between TAZ activity and drug penetration into the organoids (Supporting Fig. S9C).

Finally, to clarify the causal relationship between stromal activation by YAP/TAZ and sorafenib susceptibility in HCC, we performed experiments using SNU449-MCHO (YAP/TAZ-low) and Hep3B-MCHO (YAP/TAZ-high) organoids. Although sensitivity to sorafenib was not significantly different between SNU-449 and Hep3B cells in two-dimensional cultures (without stromal cells), Hep3B-MCHOs were significantly less sensitive to sorafenib than SNU449-MCHOs in three-dimensional cultures containing various types of stromal cells ($P < 0.01$; Supporting Fig. S10). These data indicate that stromal interactions induced by YAP/TAZ activity may mediate chemotherapy susceptibility in HCC. Taken together with the observed stromal activation in the TH model (Fig. 3C-E), these data strongly suggest that impaired drug penetration and reduced drug response in the context of high YAP/TAZ activity is likely mediated by stromal activation induced by YAP/TAZ.

Discussion

In this study, we demonstrated that YAP/TAZ activity in HCC contributes to stromal activation and affects drug penetration. Recent studies have shown that YAP/TAZ signaling is intimately involved in various aspects of hepatic stromal activation, including induction of liver fibrosis, activation of HSCs, and modulation of tissue architecture and angiogenesis, among others.[27,29,39] A plethora of genes involved in stromal activation are direct targets of YAP/TAZ.[40] It has been reported that stromal activation or fibrosis in pancreatic tissue delays penetration of cisplatin into tumor in a murine autochthonous model of pancreatic cancer.[41] In this latter study, penetration of cisplatin into pancreatic cancer was highly efficient in a xenograft transplantation model of pancreatic cancer that lacked stromal activation. Considering that genetically engineered mouse models better mimic the tumor microenvironment than xenograft transplantation models, this study suggests that the tumor stroma or microenvironment might affect the *in vivo* efficacy of cancer therapeutics.

In our study, the daily doses of VP and CA3 administered to mice intraperitoneally were 50 and 1 mg/kg, respectively, which have been shown to effectively suppress tumor growth in xenograft transplantation models of various types of cancer. However, these doses failed to suppress tumor growth in our autochthonous model of HCC with activated TAZ (i.e., TH model; see Fig. 3). The tumors induced in this model feature strong stromal activation, including activation of stellate cells and increased deposition of extracellular matrix components. We speculate that activation of the tumor stroma, induced by YAP/TAZ, likely contributed to the impaired delivery of drugs into tumors. In contrast to the TH model, the S7HM model, an autochthonous model of HCC with low YAP/TAZ activity, exhibited basal stromal activity and an efficient delivery of VP into tumors. We also found that YAP/TAZ levels and stromal activity were correlated in clinical HCC specimens, where increased levels of collagen deposition and stromal gene expression were found in tumors with activated YAP/TAZ.

To better understand the mechanism underlying impaired drug delivery into HCC, we employed MCHO models. Consistent with our *in vivo* study, Hep3B-MCHOs, an organoid tumor model with high YAP/TAZ activity, showed activation of stroma and impaired drug delivery into the organoid. Notably, suppression of YAP/TAZ in HCC cells led to significantly decreased expression of the stromal genes, α-SMA and Col1A1, in MCHOs and increased drug penetration into the MCHOs. The finding of efficient drug penetration into Hep3B-only organoids lacking stromal cells further supports the interpretation that YAP/TAZ activity in HCC impairs drug penetration into tumors through induction of stromal activation. Notably, Hep3B organoids containing WI38 cells (fibroblasts) showed significantly lower drug uptake compared with organoids containing other types of stromal cells (Supporting Fig. S9). These suggest that suppression of fibroblasts in HCC with a high YAP/TAZ activity could enhance the efficacy of cancer therapeutics such as sorafenib through surmounting physiological barriers.

In summary, high YAP/TAZ activity in tumor cells impairs drug delivery into the tumor, posing a serious challenge for molecular targeted therapies against HCC with activated YAP/TAZ signaling. Disrupting or targeting the tumor stroma might improve drug delivery into HCC with elevated YAP/TAZ activity and lead to a better response to cancer therapeutics in patients with HCC.[42]

Author Contributions: K.C., S.W.R., J.Y.P., and D.Y.K. were responsible for conceptualization. K.C., S.W.R., H.M., J.Y.P., and D.Y.K. were responsible for methodology. K.C., S.W.R., H.M., S.H., H.R.K., and H.W.L. were responsible for investigation. K.C., S.W.R., H.W.L., J.Y.P., and D.Y.K. were responsible for writing (review and editing). J.Y.P. and D.Y.K. were responsible for funding acquisition. H.W.L., S.H.A., J.Y.P., and D.Y.K. were responsible for resources. S.W.R., J.Y.P., and D.Y.K. were responsible for supervision.

REFERENCES

1) Sayiner M, Golabi P, Younossi ZM. Disease burden of hepatocellular carcinoma: a global perspective. Dig Dis Sci 2019;64:910-917.
2) Lee HW, Cho KJ, Park JY. Current status and future direction of immunotherapy in hepatocellular carcinoma: what do the data suggest? Immune Netw 2020;20:e11.
3) Wang Z, Li Z, Ye Y, Xie L, Li W. Oxidative stress and liver cancer: etiology and therapeutic targets. Oxid Med Cell Longev 2016;2016:7891574.
4) Llovet JM, Montal R, Sia D, Finn RS. Molecular therapies and precision medicine for hepatocellular carcinoma. Nat Rev Clin Oncol 2018;15:599-616.
5) Keating GM. Sorafenib: a review in hepatocellular carcinoma. Target Oncol 2017;12:243-253.

6) Zanconato F, Cordenonsi M, Piccolo S. YAP/TAZ at the roots of cancer. Cancer Cell 2016;29:783-803.
7) Nguyen CDK, Yi C. YAP/TAZ signaling and resistance to cancer therapy. Trends Cancer 2019;5:283-296.
8) Kim MH, Kim J. Role of YAP/TAZ transcriptional regulators in resistance to anti-cancer therapies. Cell Mol Life Sci 2017;74:1457-1474.
9) **Moon H**, **Cho K**, Shin S, Kim DY, Han KH, Ro SW. High risk of hepatocellular carcinoma development in fibrotic liver: role of the hippo-YAP/TAZ signaling pathway. Int J Mol Sci 2019;20:581.
10) Lee DH, Park JO, Kim TS, Kim SK, Kim TH, Kim MC, et al. LATS-YAP/TAZ controls lineage specification by regulating TGFβ signaling and Hnf4α expression during liver development. Nat Commun 2016;7:11961.
11) Yimlamai D, Christodoulou C, Galli G, Yanger K, Pepe-Mooney B, Gurung B, et al. Hippo pathway activity influences liver cell fate. Cell 2014;157:1324-1338.
12) Yi J, Lu LI, Yanger K, Wang W, Sohn BH, Stanger BZ, et al. Large tumor suppressor homologs 1 and 2 regulate mouse liver progenitor cell proliferation and maturation through antagonism of the coactivators YAP and TAZ. Hepatology 2016;64:1757-1772.
13) Van Haele M, Moya I, Karaman R, Rens G, Snoeck J, Govaere O, et al. YAP and TAZ heterogeneity in primary liver cancer: an analysis of its prognostic and diagnostic role. Int J Mol Sci 2019;20:638.
14) Santinon G, Brian I, Pocaterra A, Romani P, Franzolin E, Rampazzo C, Bicciato S, et al. dNTP metabolism links mechanical cues and YAP/TAZ to cell growth and oncogene-induced senescence. EMBO J 2018;37:e97780.
15) Wu T, Dai Y. Tumor microenvironment and therapeutic response. Cancer Lett 2017;387:61-68.
16) Martin JD, Fukumura D, Duda DG, Boucher Y, Jain RK. Reengineering the tumor microenvironment to alleviate hypoxia and overcome cancer heterogeneity. Cold Spring Harb Perspect Med 2016;6:a027094.
17) Khazali AS, Clark AM, Wells A. Inflammatory cytokine IL-8/CXCL8 promotes tumour escape from hepatocyte-induced dormancy. Br J Cancer 2018;118:566-576.
18) Luo Z, Wang Q, Lau WB, Lau B, Xu L, Zhao L, et al. Tumor microenvironment: the culprit for ovarian cancer metastasis? Cancer Lett 2016;377:174-182.
19) Aronovich EL, McIvor RS, Hackett PB. The Sleeping Beauty transposon system: a non-viral vector for gene therapy. Hum Mol Genet 2011;20:R14-R20.
20) Chen X, Calvisi DF. Hydrodynamic transfection for generation of novel mouse models for liver cancer research. Am J Pathol 2014;184:912-923.
21) **Ju HL**, **Ahn SH**, **Kim DY**, Baek S, Chung SI, Seong J, et al. Investigation of oncogenic cooperation in simple liver-specific transgenic mouse models using noninvasive *in vivo* imaging. PLoS One 2013;8:e59869.
22) Moon H, Ju HL, Chung SI, Cho KJ, Eun JW, Nam SW, et al. Transforming growth factor-β promotes liver tumorigenesis in mice via up-regulation of snail. Gastroenterology 2017;153:1378-1391.e6.
23) Verdaasdonk JS, Lawrimore J, Bloom K. Determining absolute protein numbers by quantitative fluorescence microscopy. Methods Cell Biol 2014;123:347-365.
24) Zhou L, Jiang Y, Tan A, Greenlee AR, Shen Y, Liu L, et al. Silencing of N-Ras gene expression using shRNA decreases transformation efficiency and tumor growth in transformed cells induced by anti-BPDE. Toxicol Sci 2008;105:286-294.
25) Frith CH, Ward JM, Turusov VS. Tumours of the liver. IARC Sci Publ 1994;223-269.
26) Liu-Chittenden Y, Huang B, Shim JS, Chen Q, Lee SJ, Anders RA, et al. Genetic and pharmacological disruption of the TEAD-YAP complex suppresses the oncogenic activity of YAP. Genes Dev 2012;26:1300-1305.
27) Song S, Xie M, Scott AW, Jin J, Ma L, Dong X, et al. A novel YAP1 inhibitor targets CSC-enriched radiation-resistant cells and exerts strong antitumor activity in esophageal adenocarcinoma. Mol Cancer Ther 2018;17:443-454.
28) Chen R, Zhu S, Fan XG, Wang H, Lotze MT, Zeh HJ, et al. High mobility group protein B1 controls liver cancer initiation through yes-associated protein -dependent aerobic glycolysis. Hepatology 2018;67:1823-1841.
29) Song Y, Fu J, Zhou M, Xiao L, Feng X, Chen H, et al. Activated hippo/yes-associated protein pathway promotes cell proliferation and anti-apoptosis in endometrial stromal cells of endometriosis. J Clin Endocrinol Metab 2016;101:1552-1561.
30) Yu FX, Luo J, Mo JS, Liu G, Kim Y, Meng Z, et al. Mutant Gq/11 promote uveal melanoma tumorigenesis by activating YAP. Cancer Cell 2014;25:822-830.
31) Lu T, Li Z, Yang Y, Ji W, Yu Y, Niu X, et al. Corrigendum to "The Hippo/YAP1 pathway intersects with FGFR1 signaling to maintain stemness in lung cancer" [Canc. Lett. 423 (2018) 36-46]. Cancer Lett 2018;431:244.
32) Bhavsar C, Momin M, Khan T, Omri A. Targeting tumor microenvironment to curb chemoresistance via novel drug delivery strategies. Expert Opin Drug Deliv 2018;15:641-663.
33) Nandigama R, Upcin B, Aktas BH, Ergün S, Henke E. Restriction of drug transport by the tumor environment. Histochem Cell Biol 2018;150:631-648.
34) Fateye B, Wan A, Yang X, Myers K, Chen B. Comparison between endothelial and tumor cells in the response to verteporfin-photodynamic therapy and a PI3K pathway inhibitor. Photodiagnosis Photodyn Ther 2015;12:19-26.
35) Zhang N, Zhao F, Zou Q, Li Y, Ma G, Yan X. Multitriggered tumor-responsive drug delivery vehicles based on protein and polypeptide coassembly for enhanced photodynamic tumor ablation. Small 2016;12:5936-5943.
36) **Mannaerts I**, **Leite SB**, Verhulst S, Claerhout S, Eysackers N, Thoen LFR, et al. The Hippo pathway effector YAP controls mouse hepatic stellate cell activation. J Hepatol 2015;63:679-688.
37) Wang X, Zheng ZE, Caviglia JM, Corey KE, Herfel TM, Cai B, et al. Hepatocyte TAZ/WWTR1 promotes inflammation and fibrosis in nonalcoholic steatohepatitis. Cell Metab 2016;24:848-862.
38) Padera TP, Stoll BR, Tooredman JB, Capen D, di Tomaso E, Jain RK. Pathology: cancer cells compress intratumour vessels. Nature 2004;427:695.
39) **Yui S**, **Azzolin L**, Maimets M, Pedersen MT, Fordham RP, Hansen SL, et al. YAP/TAZ-dependent reprogramming of colonic epithelium links ECM remodeling to tissue regeneration. Cell Stem Cell 2018;22:35-49.e7.
40) Zanconato F, Cordenonsi M, Piccolo S. YAP and TAZ: a signalling hub of the tumour microenvironment. Nat Rev Cancer 2019;19:454-464.
41) Olive KP, Jacobetz MA, Davidson CJ, Gopinathan A, McIntyre D, Honess D, et al. Inhibition of Hedgehog signaling enhances delivery of chemotherapy in a mouse model of pancreatic cancer. Science 2009;324:1457-1461.
42) Belli C, Trapani D, Viale G, D'Amico P, Duso BA, Della Vigna P, et al. Targeting the microenvironment in solid tumors. Cancer Treat Rev 2018;65:22-32.

Author names in bold designate shared co-first authorship.

Supporting Information

Additional Supporting Information may be found at onlinelibrary.wiley.com/doi/10.1002/hep.32000/suppinfo.